Journal of the Earth and Space Physics
Homepage: https://jesphys.ut.ac.ir
Vol. 51, No. 4, Winter 2026, P. 189-206
(Research Article)

Observed impacts of Tropical Cyclones Paddy (2021) and Freddy (2023) on the oceanic conditions in the Southeast Indian Ocean

Wijaya, Y. J.[1] ✉ | Arum, N. C.[1] | Wisha, U. J.[2,3] | Maslukah, L.[1] | Satriadi, A.[1] | Lukman, A. A.[1] | Kunarso, K.[1]

1. Department of Oceanography, Faculty of Fisheries and Marine Science, Diponegoro University, Semarang, Indonesia.
2. Coastal Processes Research Group, Research Center for Oceanography, National Research and Innovation Agency (BRIN), Jakarta, Indonesia.
3. Department of Physics and Earth Sciences, University of the Ryukyus, Nishihara, Japan.

Corresponding Author E-mail: yusuf.jatiwijaya@live.undip.ac.id

(Received: 2 Sep 2025, Revised: 1 Nov 2025, Accepted: 30 Dec 2025, Published online: 17 March 2026)

Abstract
Tropical Cyclones (TC) Paddy and Freddy traversed the southern coast of Indonesia, each exhibiting distinct intensities and times. TC Paddy occurred in November 2021, while TC Freddy occurred in February 2023. This study utilized satellite data from multiple sources to assess the variations in the effects of TCs on aquatic environments, incorporating wind, chlorophyll-a (Chl-a), and sea surface temperature (SST) data. Both TC Paddy and Freddy exhibited comparable effects on the surface waters they traversed, specifically elevated Chl-a concentrations and a reduction in SST. Interestingly, a less significant rise in Chl-a, was observed as a consequence of TC Freddy, which was characterized by stronger winds than TC Paddy. This can be partly explained by the difference in translation speed between the two TCs. TC Paddy exhibited a slower translation speed of 1.07 m/s, in contrast to TC Freddy's 4.28 m/s, leading to prolonged turbulence of the surface water influenced by TC Paddy, hence facilitating a greater uplift of nutrients to the surface. The surface currents were also affected by the translation speed parameter. The strength would be affected by the slower (faster) translation speed, resulting in a stronger (weaker) outcome. Meanwhile, for wave parameters, the TC with greater (lesser) intensity produced higher (lower) significant wave heights.

Keywords: Tropical Cyclone; Chl-a; SST; Wave; South of Java.

1. Introduction

The southern coast of Java, part of the Indian Ocean, represents an area characterized by diverse interactions among regional and global factors (Wijaya et al., 2024). The waters are affected by various oceanographic and atmospheric phenomena, including the Indonesian Through-flow (Lubis et al., 2025; Feng et al., 2018), upwelling (Wen et al., 2023; Wirasatriya et al., 2020), the South Equatorial Current, South Java Current (Wijaya et al., 2023; Ningsih et al., 2021), and tropical cyclones (TCs) (Setiawan et al., 2021). TCs are natural events that induce weather disturbances along their path, resulting in strong winds and maritime storms that affect coastal regions (Li et al., 2025; Kropf et al., 2025; Jullien et al., 2024). TCs require high sea surface temperatures (SST), instability, and profound moist convection for development and intensification (Sahoo and Bhaskaran, 2017; McTaggart-Cowan et al., 2015).

TCs infrequently make landfall in Indonesia; nevertheless, their activity at southern latitudes can significantly affect water conditions south of Java by modifying surface wind patterns, elevating wave heights, altering SST, and disrupting current circulation (Yang et al., 2024; Dac Da et al., 2023; Hendra et al., 2020; Hadi et al., 2019). Research by Susilohadi et al. (2018) showed that significant wave height in southern Java exceeding 3 meters isoften associated with TC activity in the southern Indian Ocean, particularly between November and April. Furthermore, global climate change, which affects the patterns of TC formation, is expected to increase both the frequency and

Cite this article: Wijaya, Y. J., Arum, N. C., Wisha, U. J., Maslukah, L., Satriadi, A., Lukman, A. A., & Kunarso, K.1 (2026). Observed impacts of Tropical Cyclones Paddy (2021) and Freddy (2023) on the oceanic conditions in the Southeast Indian Ocean. *Journal of the Earth and Space Physics*, 51(4), 189-206. DOI: http//doi.org/10.22059/jesphys.2025.401391.1007719

E-mail: (1) nunik.corvia09@gmail.com | lilikmaslukah@lecturer.undip.ac.id | alfisatriadi@lecturer.undip.ac.id | aulialukman@lecturer.undip.ac.id | kunarso@lecturer.undip.ac.id (2,3) ulun002@brin.go.id

Publisher: University of Tehran Press.
DOI: http//doi.org/10.22059/jesphys.2025.401391.1007719
Print ISSN: 2538-371X
Online ISSN: 2538-3906

intensity of extreme waves in this region (Hadi et al., 2019).

A TC is distinguished by the presence of powerful winds that have the potential to promote the mixing of different layers of the ocean, which in turn enriches surface waters with nutrients. This results in an increase in the concentrations of chlorophyll-a (Chl-a) in the regions that are brought under the influence of the cyclone (Shi et al., 2025; Chen et al., 2022; Li and Tang, 2022; Liu et al., 2020; Chacko, 2019). For instance, Efendi, (2018) reported that Chl-a variability in southern Java surged by 88-100% one-week post-cyclone. Furthermore, Setiawan et al., (2021) conducted study indicating that Chl-a and sea surface temperature (SST) in the Savu Sea were affected by wind speed and the translational speed of TC Seroja. Setiawan et al. (2021) have also indicated a positive association between TC and Chl-a within Indonesian territory, attributed to upwelling and mixing processes.

In late November 2021, BMKG detected and reported a tropical storm in the Indian Ocean south of Central Java, identified as TC Paddy, at a velocity of 20 m/s. The cyclone advanced westward at a velocity of 5 km/h, distancing itself from Indonesian territory, resulting in heavy to moderate rainfall across several regions (Pattie, 2022). In mid-February 2023, another TC, designated as Freddy, manifested in the Indian Ocean south of Bali, reaching a maximum intensity of 38 m/s. The cyclone progressed southwest, departing from Indonesian territory (Ciardullo et al., 2025; Liu et al., 2023). The interaction dynamics between two distinct TC significantly influence the physical and biogeochemical conditions of marine waters. This aspect is crucial in the study of ocean-atmosphere interactions due to its potential for redistributing water masses, mixing ocean layers, and affecting primary productivity and marine ecosystems. In this study, we endeavor to determine the extent to which the water conditions in southern Java varied prior to, during, and following the passage of TC Paddy and Freddy. We aim to accomplish these objectives by utilizing reanalysis data and high-resolution satellite data that are currently available. Data on Chl-a, SST, wind, significant wave height, and surface current were utilized in this study.

2. Materials and Methods

2-1. Data

The geographical boundaries of the research region are located in the Indian Ocean, just south of Java Island, extending from 105˚ to 115˚E and from 5˚ to 20˚S (see Figure 1). The data utilized encompasses each TC during a one-month period, including the pre-cyclone phase, the peak of cyclone itself, and the post-tropical cyclone phase. TC Paddy traversed the southern region of Java Island in November 2021, while TC Freddy occurred in February 2023. This investigation makes use of satellite data obtained from a variety of different sources. The variables and data sources employed in this study are summarized in Table 1.

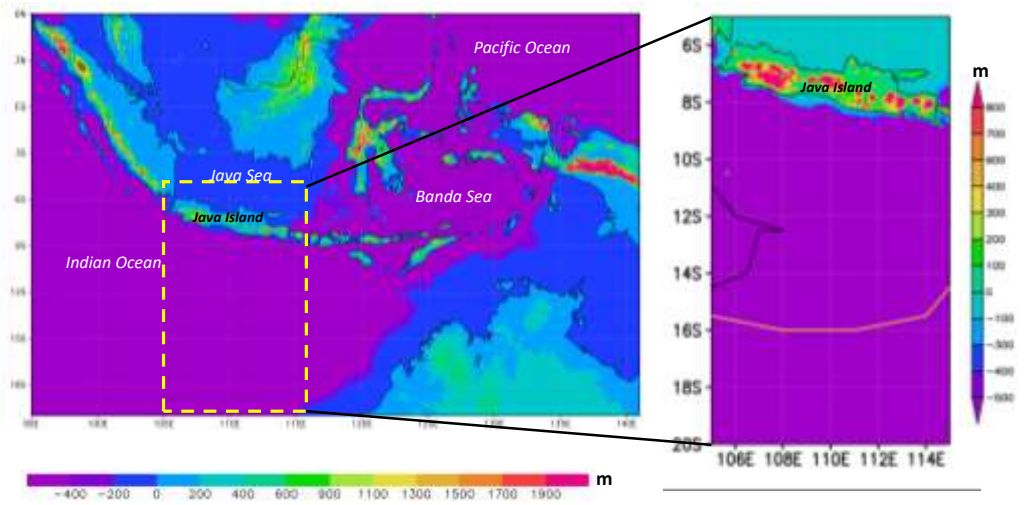

Figure 1. The observation region is marked by dotted yellow box. The black and yellow lines in the right panel denote the trajectories of TC Paddy and Freddy, respectively.

To comprehend the physical features of TC Paddy and Freddy, we utilized surface wind data acquired from the Cross-calibrated Multi-platform (CCMP). Suzuki et al. (2018) evaluated multiple wind speed dataset sources and determined that the CCMP dataset exhibited the highest accuracy. However, the current version of CCMP demonstrates considerable accuracy at wind velocities below 15 m/s but tends to underestimate wind speeds at greater magnitudes (Mears et al., 2019). The wind dataset shares a spatial resolution of 0.25 degrees in both latitude and longitude for the u and v components. The CCMP dataset provides temporal resolution at intervals of six hours each. Comprehensive specifications, data assimilation techniques, and further information regarding the CCMP data are available in the works of Atlas et al. (2011).

The European Space Agency supervises the Ocean-Color Climate Change Initiative (OC-CCI) project, which gathered the Chl-a data included in this study. The Chl-a data can be freely downloaded from the Marine Copernicus website at this address: http://marine.copernicus.eu/. The data is accessible at a daily temporal period and a spatial resolution of 4×4 km (Sathyendranath et al., 2019). The OC-CCI algorithm is designed for use in the open ocean environment. In turbid waterways, dissolved organic matter, sediment, and dust particles result in a persistent overestimation, as the spectral signal is not only derived from chlorophyll (Goncalves-Araujo et al., 2018).

Furthermore, data on the SST that came from the Operational Sea Surface Temperature and Sea Ice Analysis (OSTIA) were also utilized in this study. The OSTIA system is responsible for the generation of SST data through the use of in-situ and satellite measurements. It comes with a spatial resolution of 1/20 degree and a daily temporal resolution. Free access to SST data from OSTIA is available on the Marine Copernicus website. Good et al. (2020) and Donlon et al. (2011) provide a comprehensive examination of the properties of these data. The data on SST were utilized in order to determine the changes in the impact that TC Freddy and Paddy had on the cooling of the aquatic environment that they got through.

In addition, this study employed reanalysis data on significant wave heights (SWH), sea water temperature (SWT), and surface currents, sourced from Marine Copernicus. Surface current and SWT data were derived from the GLORYS12V1 product, featuring a horizontal resolution of 0.083º (Lellouche, et al., 2013). The GLORYS12 sea level is approximately 0.25 mm lower than the altimetry annually (Jean-Michel et al., 2021). This bias primarily arises from the standard utilized for the orbit. We utilized SWH data from WAVERYS, including a geographical resolution of 0.2º and a temporal resolution of every 3 hours. There is a slight bias for global products and the SWH scatter index averages 8% with better data assimilation. Comprehensive and extensive information pertaining to data specifications is available in the work by Ardhuin et al. (2010).

Table 1. Overview of the data utilized in the research.

No	Variables	Source	Spatial resolution
1	Wind speed	the Cross-calibrated Multi-platform (CCMP)	0.25˚
2	Chl-a	the Ocean-Color Climate Change Initiative (OC-CCI)	4 km
3	SST	the Operational Sea Surface Temperature and Sea Ice Analysis (OSTIA)	0.05˚
4	Significant wave height	WAVERYS	0.2˚
5	Surface current	GLORYS12V1	0.083˚
6	Sea water temperature	GLORYS12V1	0.083˚

2-2. Data Analysis

Wind data acquired from CCMP will be analyzed utilizing the methods provided below to derive values for wind speed, wind stress curl (WSC), and Ekman pumping velocity (EPV). Each of these variables played a crucial role in defining the physical properties of TC and the way TC interacts with surface water. Initially, the wind speed is calculated using Equation (1):

$$V = \sqrt{(u^2 + v^2)} \ldots \quad \ldots..(1)$$

in which u and v represent the zonal and meridional components of wind, respectively. West-east direction is zonal, while south-north direction is meridional.

Subsequently, by utilizing the u and v components of the wind data, we transformed them into WSC through the application of Equation (2):

$$\mathrm{WSC} = \frac{\partial \tau_y}{\partial x} - \frac{\partial \tau_x}{\partial y} \ldots\ldots \quad ..(2)$$

where τ_x and τ_y are the wind stress components derived from Equations (3) and (4) as presented by Kok et al. (2017) and Kutsuwada (1998):

$$\tau_x = \rho_\alpha C d V u \ldots\ldots \quad ..(3)$$

$$\tau_y = \rho_\alpha C d V v \ldots\ldots \quad ..(4)$$

where ρ_α represents the density of air, which is 1.2 kg/m³, and Cd denotes the drag coefficient, valued at about1.3×10^{-3}.

Wind data was also utilized to compute EPV, facilitating the analysis of the vertical movement of water masses influenced by TC Freddy and Paddy. According to the findings presented by Wirasatriya et al. (2020), the calculation of EPV was conducted in Equations (5) and (6):

$$\mathrm{EPV} = -\frac{\mathrm{WSC}}{\rho_w f} \ldots \quad \ldots..(5)$$

$$f = 2\Omega \sin \varphi \ldots \quad ...(6)$$

In Equation (6), f represents the Coriolis factor, Ω denotes the Earth's rotational speed, quantified as 7.29 x 10^{-5} rad/s, and φ indicates the latitude expressed in radians. In Equation (5), the density of sea water is ρ_w, which is 1025 kg/m³.

The analysis of Chl-a data produced results regarding concentration and distribution. Visualization was performed with detailed attention to the occurrences of TC Paddy during the periods of November 20-25, alongside the occurrences of TC Freddy during the intervals of February 7-12, 2023. This was likewise applicable to all data utilized as observational variables in this investigation. In order to conduct a thorough analysis of the relationship between TCs and SST and Chl-a, we computed the average of each variable prior to (November 17 to 20, 2021), during (as mentioned above), and following the occurrence of the TC Paddy (November 25 to 28, 2021). In the case of TC Freddy, the specifics are outlined as follows: before (February 4 to 7, 2023), during (as previously stated), and after the event of TC Freddy (February 12 to 15, 2023). We established a four-day window before and after the event for observation, under the assumption that the residual effects of the TC had dissipated from the observation site. Furthermore, the area was averaged over the region affected by the TC events. Considering that the location is a certain area that TC passes through. For TC Paddy, the coverage extended from 8ºS to 17ºS and from 105ºE to 110ºE. In the case of TC Freddy, the area spanned from 12ºS to 18ºS and from 105ºE to 110ºE. The data processing for this research was conducted exclusively with OpenGrads software.

3. Results and Discussion

3-1. Wind patterns observed during TC events

TC Paddy and Freddy traversed over the southern waters of Java in around six days, according to an analysis of the spatial distribution of winds shown in Figure 2. Consequently, we presented the observed variables corresponding to the temporal occurrence of the TC at the observation location boundary, specifically TC Paddy from November 20, 2021, to November 25, 2021, and TC Freddy from February 7, 2023, to February 12, 2023. Moreover, Figures 2 and 3 depict the daily visualization of wind direction and speed during TC Paddy and Freddy. The wind movement was characterized by a clockwise direction, with low wind speeds at the cyclone's center and higher wind speeds in the surrounding area. This represents a common occurrence of a TC in the southern hemisphere (Pillay and Fitchett, 2020, 2021). Both the movement and intensity features of the two TC are extremely different from one another.

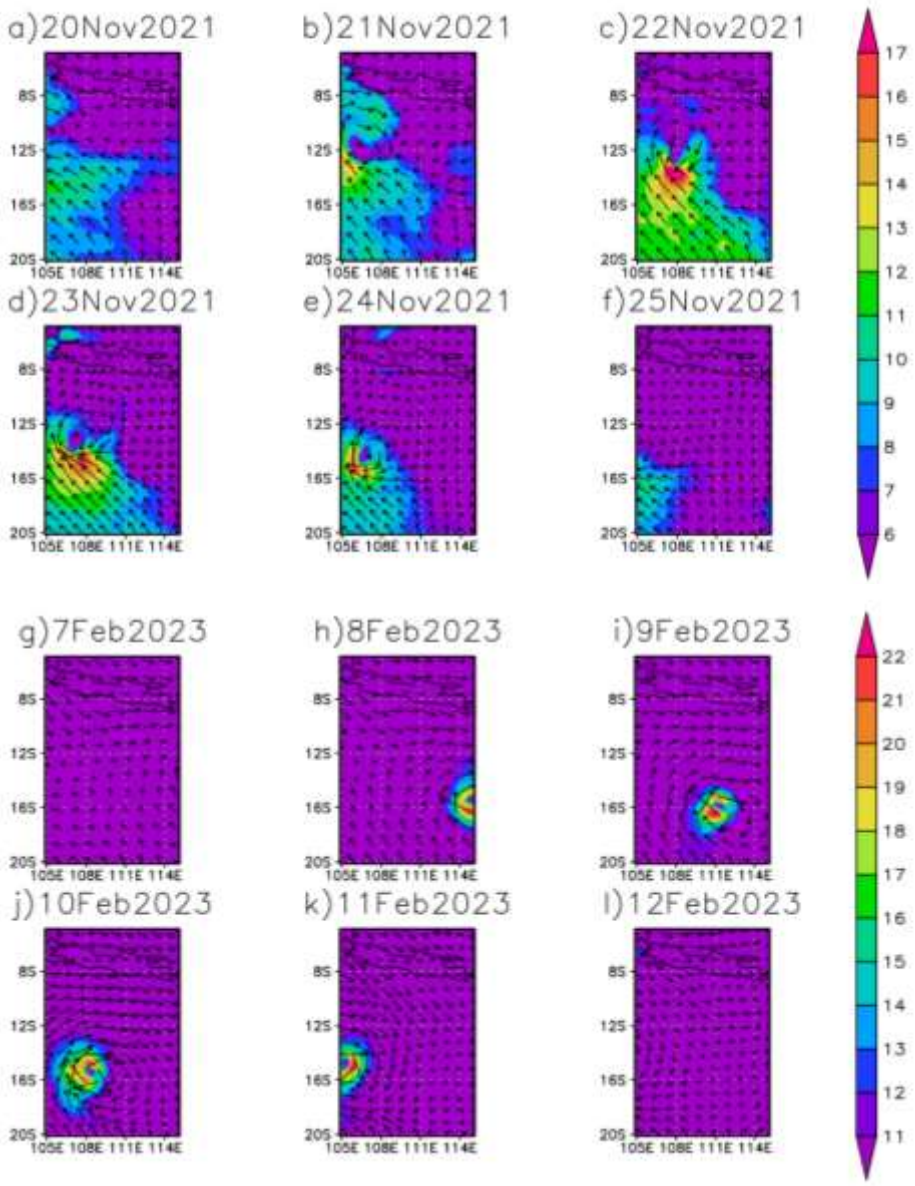

Figure 2. Surface wind patterns during the TC paddy in 2021 are illustrated in Figures (a) to (f). Figures (g) to (l) depict the surface wind conditions during TC Freddy in 2023. The vector denotes wind direction, but the color signifies magnitude in m/s.

TC Paddy's seed developed outside our specified observation area, located in the southwestern region of Java. Subsequently, it progressed gradually eastward without notable development, beginning to encroach into the observation area on November 21, 2021. TC Paddy transitioned into the TC phase on November 22, 2021, reaching its peak intensity on the same day and categorizing as a system of category 1 (as per the classifications used by the Australian Bureau of Meteorology). TC Paddy progressively advanced southwestward within the observation area from November 22 to November 24. The strongest sustained winds were seen in the southern system of the TC Paddy structure, with gusts hitting 17 m/s. Nevertheless, this condition was transient; the system exhibited a slow decline on November 23 and 24, 2021, and was no longer detectable at the observation areaon November 25, 2021 (Pattie, 2022).

For TC Freddy, the tropical depression initiated formation in the eastern region of the observation area, specifically to the south of the Lesser Sunda Islands (Perry et al., 2024). This condition eventually evolved into a TC on February 6, 2023, as documented by Liu et al. (2023). Subsequently, it progressed gradually westward, where on February 7, TC Freddy had not yet traversed the waters

south of Java (Figure 3a). TC Freddy showed up in the observation area on February 8, with maximum wind speeds surpassing 22 m/s (Figure 3b). Between February 8 and 11 (Figure 3b-3e), TC Freddy's structure remained mostly stable while traversing the southern waters of Java, despite the diameter of its wind gusts, seemed to expand on 10 February 2023. Afterwards, the cyclone became undetectable within the observation area (Figure 3f), it shifted southwestward toward Madagascar, ultimately establishing a record as the most enduring TC (Perry et al., 2024).

3-2. Response of SST and Chl-a during TC Events

Numerous prior studies have demonstrated that the passage of TCs over an ocean results in a reduction of SST by as much as 2˚C (Yu et al., 2023; Dare and McBride, 2011). It is important to highlight that TC necessitate SST exceeding 25.5˚-26.5˚C for their formation and sustenance of intensity (Tory and Dare, 2015; McTaggart-Cowan et al., 2015). Therefore, to assess the impact of TCs on the ocean, we investigated the time series of SST when the TCs were identified within the observation region. Figure 3 indicates that prior to the TC traversing the southern waters of Java, SSTs varied between 26.5˚ and 29˚C. This aligns with previous study, which found that the average sea surface temperature in southern Java ranged from 26°C to 29.5°C (Wijaya et al., 2024; Wirasatriya et al., 2020). This situation enabled TC to sustain its intensity while entering southern Java.

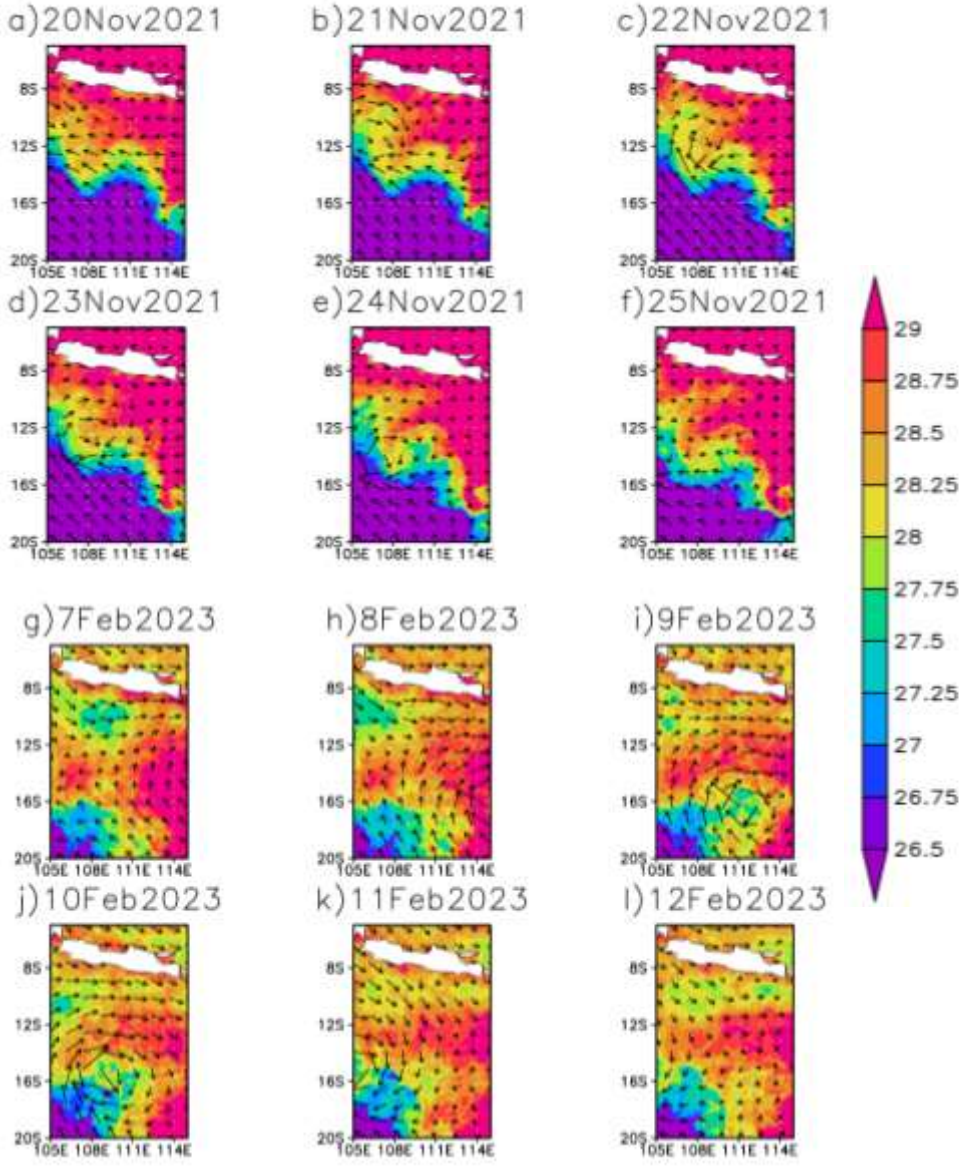

Figure 3. Same as Figure 2, but for the distribution of SST in ºC.

Following the entry of TC Paddy into the observation region from the west between November 21 and 23, 2021 (Figure 3b-3e), the SST in the vicinity of latitude 10°S to 13°S dropped by roughly 0.5°C. This result remained below the global average reported by Dare and McBride (2011), which indicated that the SST decline had reached 0.9°C. After the TC departed from the waters south of Java, SST was observed to rise, ultimately reaching 29°C at the same latitude (Figure 3f). In the southern region of the observation area, interesting phenomena were observed; specifically, the TC on November 24 resulted in an increase in SST around latitude 14° to 15°S. The increase was somewhere between 0.25° and 0.5°C. It was a rare occurrence; however, it was plausible that intensified winds are pushing warmer water masses southward from latitudes north of 13°S, leading to an elevation in SST.

For TC Freddy, SST values around the path of TC encountered a decrease of approximately 1°C to 2°C. The decline of SST commenced on February 9, 2023, as TC Freddy had not yet entirely entered the observation area on February 8, and was still located south of Bali. From February 10 to 12, the SST in the vicinity of latitudes 14° to 17°S experienced a cooling due to the linear movement of TC Freddy from east to west. Following the TC's departured from the southern waters of Java on February 12, the SST resumed increases. The reduction in SST along the trajectory of a TC is sometimes ascribed to a phenomena termed a cold wake. This phenomena transpired when the intense winds linked to a TC blended warm surface water with colder subsurface layers, leading to an overall reduction in surface temperature (Yan et al., 2025; Akhila et al., 2022; Karnauskas et al., 2021).

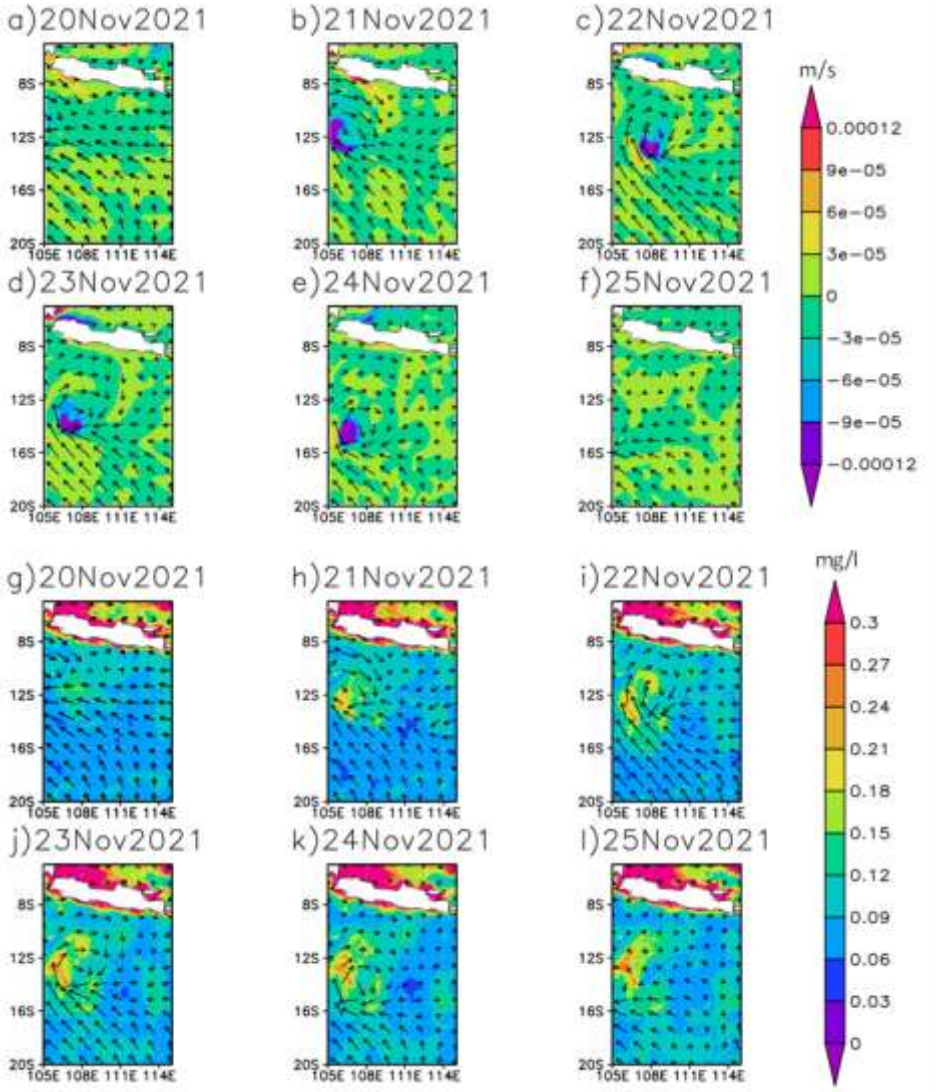

Figure 4. The distribution of EPV during the TC Paddy are illustrated in Figures (a) to (f). Figures (g) to (l) depict the distribution of Chl-a. The vector denotes wind direction.

TC Paddy and Freddy significantly contributed to the enhancement of Chl-a concentration via the upwelling mechanism induced by EPV along the trajectory of the TC. The results indicated that negative EPV values were consistently produced in reaction to the movement of the TC, as shown in Figures 4 and 5. Negative EPV values suggested upward velocities, signaling the occurrence of an upwelling phenomenon in the area (Setiawan et al., 2021; Wirasatriya et al., 2020). During the progression of TC Paddy, there was a notable increase in Chl-a concentration, reaching an average of 0.21 mg/l (Figures 4g to 4l). Following the passage of TC Paddy over the water, there was a gradual decline in Chl-a concentration, signifying the trajectory of the TC.

Similar patterns were observed during TC Freddy, where Chl-a concentrations rose, albeit at lower levels compared to TC Paddy (Figures 5g to 5l). During the presence of TC Freddy over a body of water, there was a notable increase in Chl-a concentration, averaging 0.12 mg/l, with a peak value recorded at 0.18 mg/l. Upon examining February 9 to 12, it was evident that the rise in Chl-a gradually diminished, yet it still retained remnants along the trajectory of TC Freddy, similarly to the occurrence of TC Paddy. Analysis of the wind speed indicated that TC Paddy exhibited a lower wind speed compared to TC Freddy; however, the concentration of Chl-a was higher during the occurrence of the TC Paddy. The phenomenon observed may be attributed to TC Paddy traversing the southern region of Java in November, coinciding with an upwelling event that resulted in a rise in Chl-a concentration in the area, albeit with a relatively slight intensity (Wijaya et al., 2024).

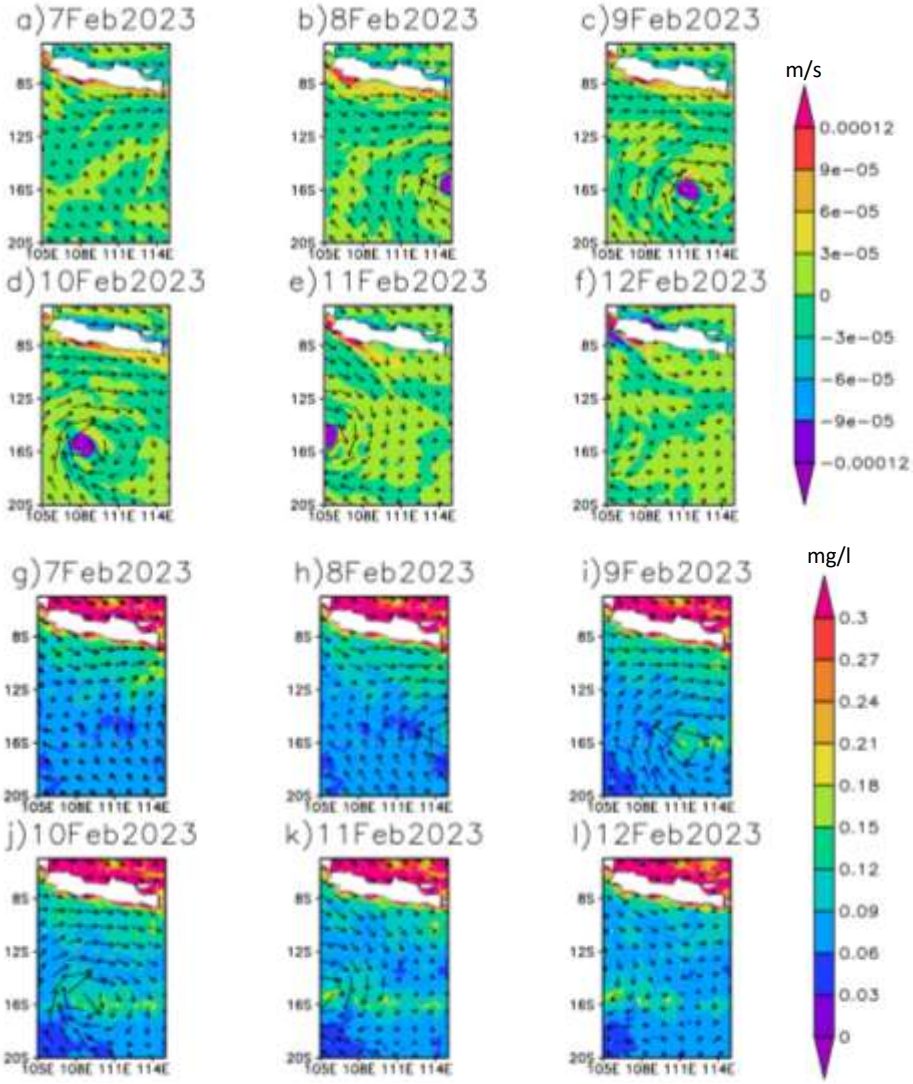

Figure 5. Similar to Figure 4, but for TC Freddy.

Vertical profiles of SWT were presented to confirm the upwelling of cold water mass from the subsurface as the TC traversed the waters south of Java. Observations concentrated on the locations where the TC attained its maximum intensity, specifically at latitudes 14ºS for Paddy and 17ºS for Freddy. Figure 6 illustrates the occurrence of a mixing process during the passage of TC Paddy and Freddy. The subsurface water mass that ascended to the surface exhibited lower temperatures during the peak of TC Freddy in February 2023. When TC Paddy occurred in November 2021, it coincided with La Nina (Huang et al., 2024; Li et al., 2023) and Negative IOD (Wijaya et al., 2024) events, resulting in increased water temperatures in southern Java. In February 2023, the triple dip La Niña that commenced in the 2020/2021 period ended (Chen et al., 2025), resulting in a cooling of SST in Indonesian waters.

Moreover, to conduct a more thorough examination of the varying impacts of TC Paddy and Freddy on the southern waters of Java, we computed the average of each variable at the designated location. The average calculations performed at each site of TC activity, taking into account the conditions before, during, and after the occurrence of TC, indicated that the Chl-a concentration was much higher during TC Paddy (Figure 7). A p-value of less than 0.05 suggests that the findings are statistically significant. Although the correlation coefficient (*r*) between wind speed and Chl-a is low (-0.1), Chl-a concentrations showed a peak as TC Paddy traversed southern Java, with the maximum average value recorded at approximately 0.125 mg/l on November 23, 2021. Prior to the TC event, the peak average Chl-a concentration was approximately 0.09 mg/l, indicating a 39% rise in Chl-a concentration. This was accompanied by a reduction in SST of 0.4˚C, which attained its minimum value of approximately 27.5˚C. This finding aligns with the study conducted by Wang et al. (2023), which showed that the TC can lead to increased Chl-a concentrations in aquatic environments via the Ekman pumping mechanism. Once the TC left the observation area, Chl-a did not instantly revert to its original minimum value, suggesting that the TC trajectory continued to manifest residual effects as evidenced by Chl-a concentrations monitored by satellites. However, this was not applicable to SST, which immediately witnessed a spike following TC Paddy. The high *r* value (-0.89) suggested that the strong gusts associated with TC Paddy resulted in a decrease in water temperature within the observation area.

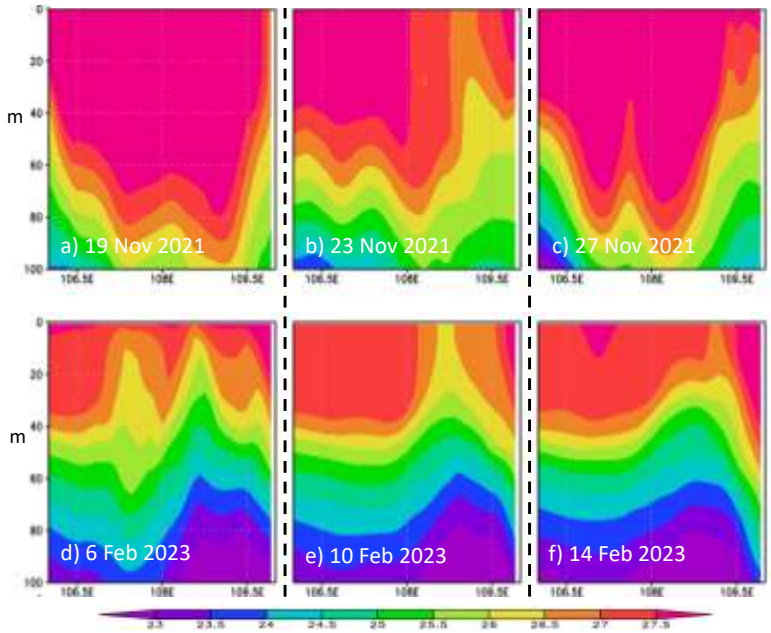

Figure 6. The upper panel displays the SWT pattern associated with TC Paddy (at 14ºS) prior to its occurrence on November 19, 2021 (a), during its occurrence on November 23, 2021 (b), and following its occurrence on November 27, 2021 (c). The lower panel depicts TC Freddy (at 17ºS) prior to its occurrence on February 6, 2023 (d), during its occurrence on February 10, 2023 (e), and following its occurrence on February 14, 2023 (f). Expressed in ºC.

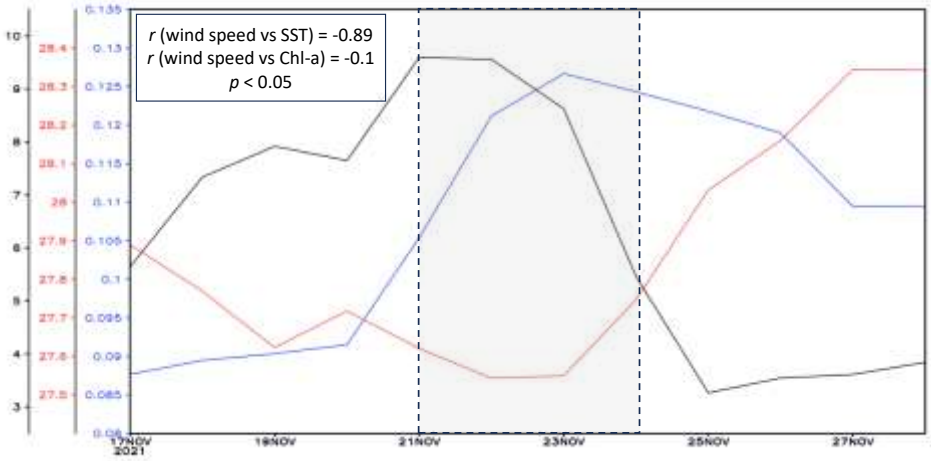

Figure 7. Area averages for wind in m/s (black line), SST in ºC (red line), and Chl-a in mg/l (blue line) throughout the pre-, during, and post-2021 TC Paddy event. Specifically between longitudes 105˚E and 110˚E, and latitudes 8˚S and 17˚S. The period during which the TC traversed the observation area was denoted by a dotted gray square.

The p-values obtained, which are less than 0.05, indicate a statistically significant relationship among the wind, SST, and Chl-a variables. However, the correlation between wind speed and SST, as well as Chl-a during TC Freddy, demonstrated results comparable to those observed during TC Paddy, with wind speed exhibiting a strong positive association with SST (-0.71) and a weak relationship with Chl-a (0.23). Figure 8 illustrates a rise in Chl-a concentration coinciding with the passage of TC Freddy across the southern waters of Java. However, the average maximum Chl-a concentration reached was around 0.093 mg/l, which was still lower than the Chl-a concentration noted during TC Paddy. The peak Chl-a concentration recorded prior to the TC event was approximately 0.072 mg/l. Hence, the rise in Chl-a during the TC Freddy event was 29.2%. This was accompanied by a reduction in SST of 0.5˚C, decreasing from 28.8˚C prior to the TC to 28.3˚C upon its entry into the observation region. The residual effect of TC Freddy on the waters was reflected in the Chl-a concentration, which remained higher along the TC path for two days before reverting to its baseline level prior to the TC event. Following the TC event, SST had an increase referred to as recovery time. Following the TC Paddy event, SST had a substantial spike, but the increase in SST following TC Freddy was quite modest. The SST decreased by 0.4°C from before to during TC Paddy, indicating a less pronounced cooling effect compared to TC Freddy. Ling et al., (2021) asserted that a prolonged (shorter) recovery time will result from stronger (weaker) SST cooling.

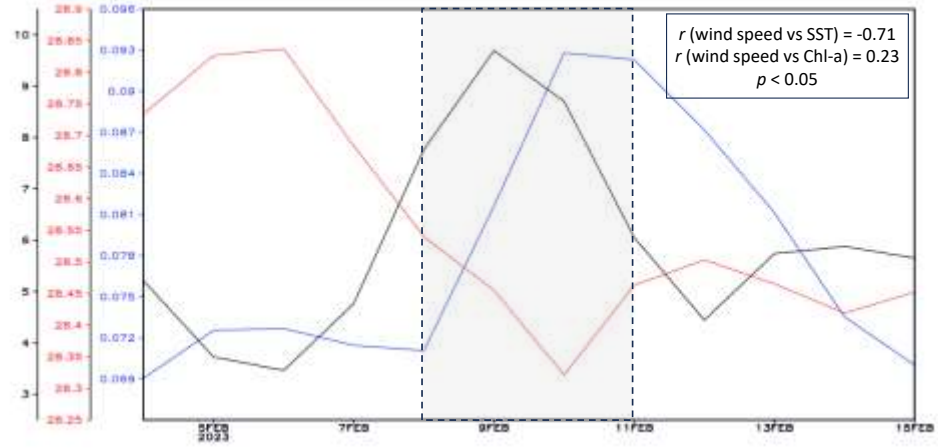

Figure 8. Area averages for wind in m/s (black line), SST in ºC (red line), and Chl-a in mg/l (blue line) throughout the pre-, during, and post-2023 TC Freddy event. Specifically between longitudes 105˚E and 115˚E, and latitudes 12˚S and 20˚S. The period during which the TC traversed the observation area was denoted by a dotted gray square.

The variation in the rise of Chl-a concentration between TC Paddy and Freddy may also be attributed to the varying translation speeds of the two. TCs that exhibited a slower translation speed were associated with greater increases in Chl-a levels (Chacko, 2019; Zhao et al., 2017). The translation speed of TC Paddy was calculated as it transitioned from latitude 12ºS to 14.5ºS between November 21 and November 24, 2021. In a separate analysis, TC Freddy's movement from longitude 115ºE to 105ºE was examined from February 8 to February 11, 2023. The findings indicated that TC Paddy exhibited a translation speed of 1.07 m/s, whereas TC Freddy achieved a speed of 4.28 m/s. The slower translation speed led to an extended duration for the mixing mechanism within a body of water, consequently allowing a greater quantity of nutrients to ascend to the surface. At the same time, a fast translation speed resulted in a shorter mixing duration in aquatic environments, consequently causing minimal elevation of Chl-a (Li and Tang, 2022; Wang, 2020; Zhao et al., 2017). Nonetheless, it is essential to take into account additional factors, including the prevailing climate conditions. In November, as TC Paddy occurred, the southeasterly monsoon was predominant in southern Java. This wind pattern has the potential to induce upwelling, facilitating the ascent of nutrient-rich deeper water to the surface, thereby increasing Chl-a concentration.

3-3. Response of Wave and Ocean Current

In addition to Chl-a, ocean waves were another variable affected by TC activities. Figure 9 demonstrates that greater SWH were produced during TC Paddy, which exhibited a more intense TC strength compared to TC Freddy. This contrasted with Chl-a, where the largest concentrations were observed during TCs with the slowest translation speed. When TC Freddy traversed southern Java, it generated SWH surpassing 5 meters. During TC Paddy, the waves attained a maximum significant height of 4 meters. Prior research indicated that greater ocean wave heights were produced by more intense TC (Sun et al., 2021; Akperov et al., 2024; Hegermiller and Thomson, 2025). Wind energy is transferred to the sea surface through friction; Young (1999) posits that wave energy is directly proportional to the square of wind speed. This implies that TCs exhibiting greater wind intensity generated higher SWH. Moreover, Zhang and Oey (2018) asserted that TCs with moderate translation speeds (3 to 7 m/s) produced larger waves compared to those with excessively rapid or slow translation speeds. This also aligns with our findings, wherein TC Freddy, exhibiting a translation speed of 4.28 m/s, generated higher SWH. The inverse barometer effect suggested that low atmospheric pressure in the middle of a TC slightly raised the sea surface. This could have an indirect effect on wave dynamics, especially near the coast where wave setup and storm surge collaboratively elevated water levels and wave impact (Jullien et al., 2024).

Figure 10 depicts the patterns of surface currents that occurred during the TC Paddy and Freddy occurrences. In comparison to TC Freddy, TC Paddy was responsible for producing surface currents that were more powerful. Even TC Paddy was capable of producing significant cyclonic eddy currents on the ocean's surface, which were less pronounced during the TC Freddy event. The results align with the Chl-a distribution pattern, wherein the cyclonic eddy signified a strong mixing process, leading to an augmentation of nutrients, which served as the primary sustenance for phytoplankton. Consequently, the concentration of Chl-a looked to be higher during TC Paddy. Ma et al. (2021) indicated that TCs capable of producing cyclonic eddy currents at the sea surface were characterized by slow translation speeds. This is consistent with our findings, which showed that TC Paddy's translation speed was comparatively slow at 1.07 m/s. In addition, TC Paddy traversed the southern waters of Java in November, a period characterized by the frequent formation of eddy currents in the area with significant strength (Zu et al., 2022). According to Lin et al. (2025), TC-induced eddy currents were a result of the intricate process of energy transfer between kinetic and potential energy.

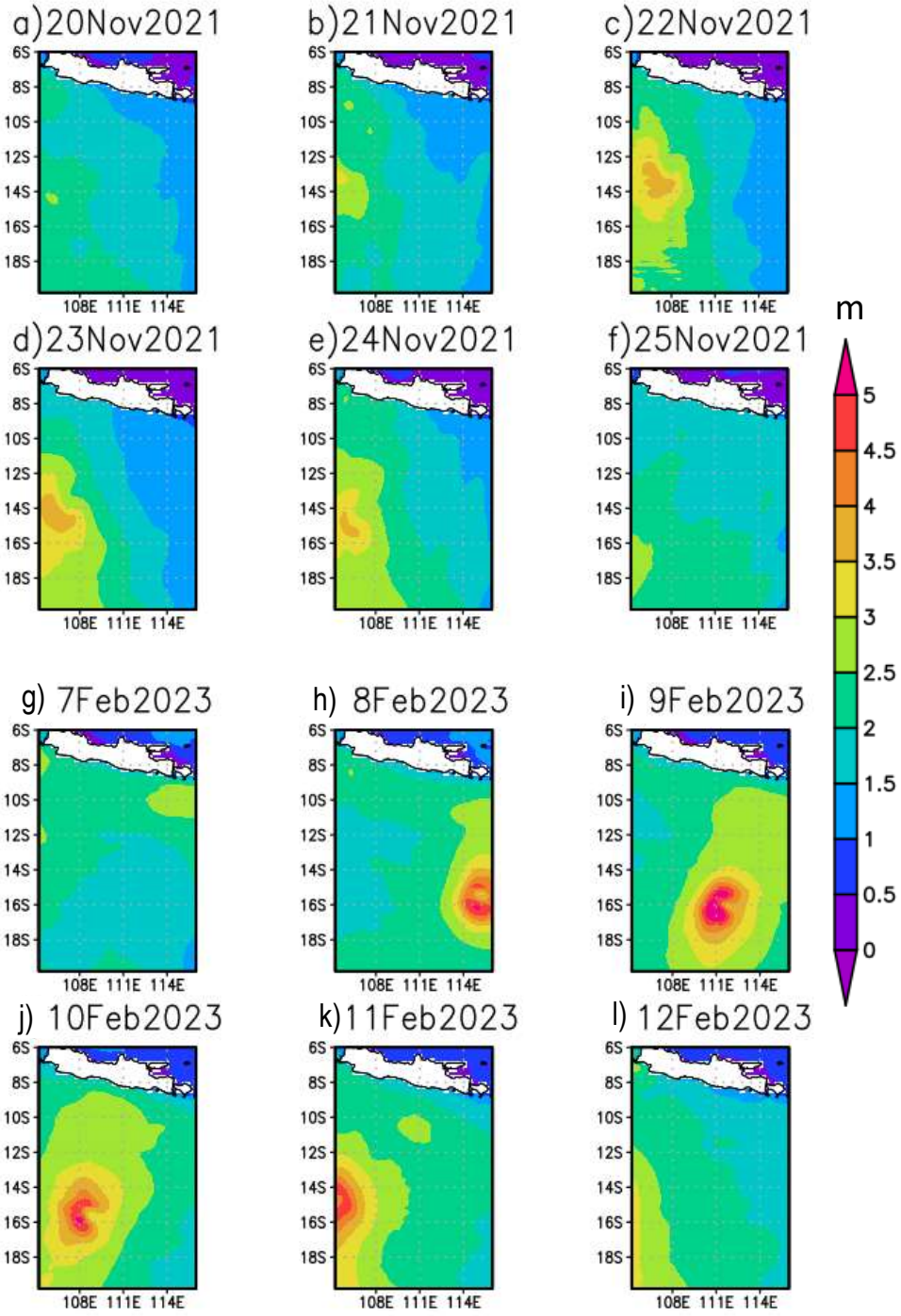

Figure 9. SWH patterns observed during TC Paddy in panels (a) to (f) and during TC Freddy in panels (g) to (l).

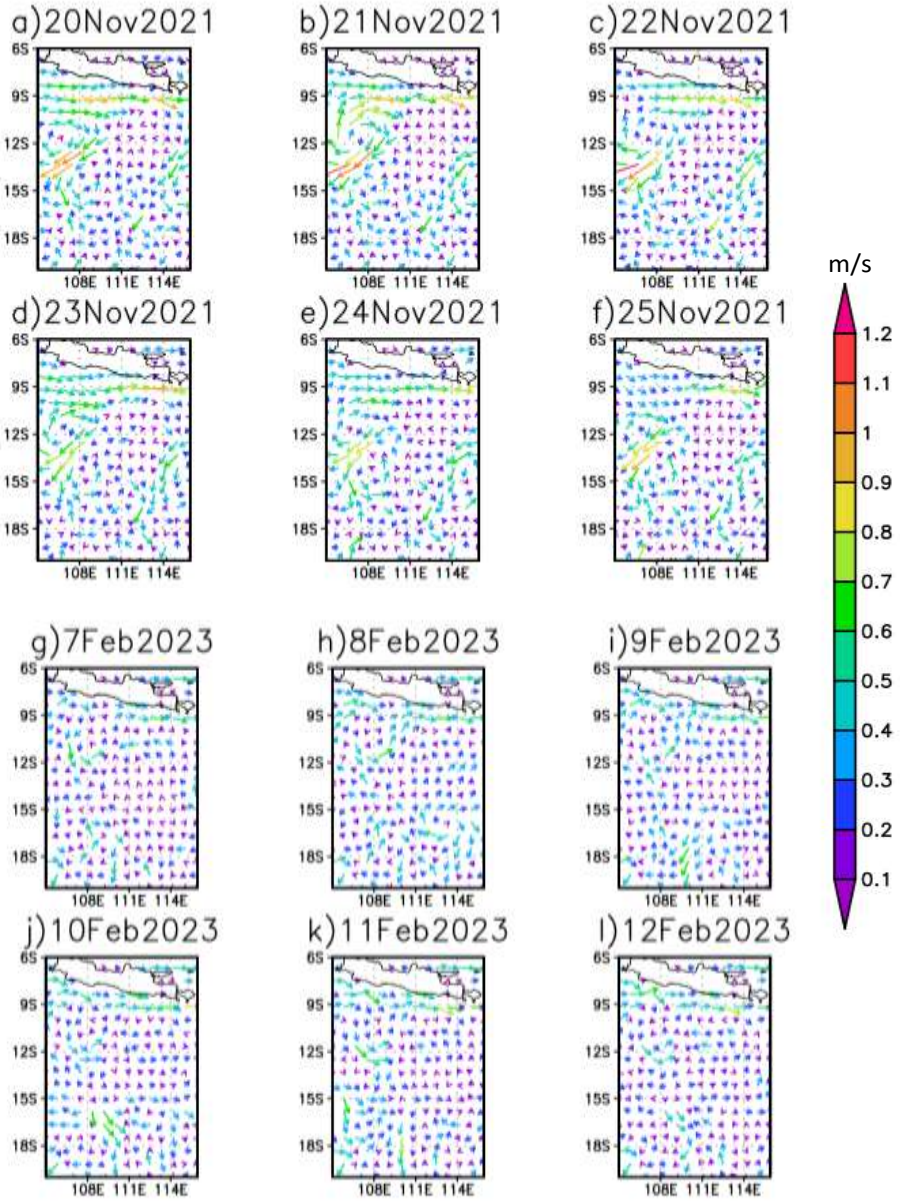

Figure 10. Similar to Figure 9, but for surface current.

4. Conclusions

TC Freddy traversed south of Java from February 8 to 11, 2023, exhibiting greater wind intensity compared to TC Paddy. Interestingly, TC Freddy, despite its stronger wind magnitude, resulted in a lesser increase in Chl-a. The increase in Chl-a concentration during the peak TC event was roughly 29%, yielding an average value of 0.093 mg/l. The difference in translation speed was explained as follows: TC Paddy travelled at 1.07 m/s, while TC Freddy reached a speed of 4.28 m/s. A slower translation speed prolonged the mixing duration in a body of water, resulting in a greater volume of water column ascending to the surface. In addition, November is the end of the upwelling season in southern Java, where Chl-a concentrations tend to be higher during that month. The water column ascended from the subsurface to the surface appeared to be cooler during the TC Freddy event. This was attributable to TC Paddy traversing southern Java in November 2021, coinciding with La Niña and negative IOD events, which contributed to the surrounding waters of Indonesia tending to be warmer. The correlation coefficient analysis further revealed an inverse relationship between wind speed and SST distribution, indicating that a more intense TC was associated with a decrease in SST

within its trajectory.

We also found that TCs exert differential influences on waves and surface currents. TC Freddy, exhibiting greater intensity, resulted in a higher SWH. In contrast, the slow-moving TC Paddy generated eddy currents on the ocean surface with strong intensity. This phenomenon was not observed during the passage of TC Freddy through southern Java. This was probably the same mechanism responsible for the greater increase in Chl-a in TC Paddy, as the extended mixing duration in slow-moving TCs provide adequate time for eddy currents to develop. Also, during the latter half of the year, eddy currents are more frequently generated in southern Java.

TCs promote vertical mixing, elevating nutrients-dense deeper water to the surface, hence enhancing primary productivity for several days. TCs take thermal energy from the ocean surface, resulting in a decrease in sea surface temperature across southern Java. This can reduce ocean heat content and affect regional climate responses. The identical cyclone will generate higher surge levels due to rising sea levels. Probabilistic hazard modeling and sea-level rise projections are critical elements of long-term preparedness.

Aknowledgements

This research is funded by the Faculty of Fisheries and Marine Sciences, Diponegoro University, under Number 19/UN7.F10/PP/III/2025.

References

Akhila R. S., Kuttippurath, J., Sarojini, B. B., Chakraborty, A., & Rahul, R. (2022). Observed tropical cyclone-driven cold wakes in the context of rapid warming of the Arabian Sea. *Journal of Operational Oceanography*, 16(3), 236–251. https://doi.org/10.1080/1755876x.2022.2068260

Akperov, M. G., Gippius, F. N., & Mokhov, I. I. (2024). Relation of Sea Waves to the Atmospheric Cyclone Activity in the Northern Hemisphere according to the ERA5 Reanalysis Data. *Russ. Meteorol. Hydrol*, 49, 195–202. https://doi.org/10.3103/S1068373924030026

Ardhuin, F., Rogers, E., Babanin, A. V., Filipot, J., Magne, R., Roland, A., et al. (2010). Semiempirical Dissipation Source functions for ocean waves. Part I: Definition, calibration, and validation. *Journal of Physical Oceanography*, 40(9), 1917–1941. https://doi.org/10.1175/2010jpo4324.1

Atlas, R., Hoffman, R. N., Ardizzone, J., Leidner, S. M., Jusem, J. C., Smith, D. K., & Gombos, D. (2010). A cross-calibrated, multiplatform ocean surface wind velocity product for meteorological and oceanographic applications. *Bulletin of the American Meteorological Society*, 92(2), 157–174. https://doi.org/10.1175/2010bams2946.1

Chacko, N. (2019). Differential chlorophyll blooms induced by tropical cyclones and their relation to cyclone characteristics and ocean pre-conditions in the Indian Ocean. *Journal of Earth System Science*, 128(7). https://doi.org/10.1007/s12040-019-1207-5

Chen, Y., Ren, C., Feng, Y., Shi, H., Pan, G., Cooper, M., & Zhao, H. (2022). Different responses of chlorophyll a to the passage of the tropical storm Wipha (2019) in the coastal waters of the northern Beibu Gulf. *Frontiers in Marine Science*, 9. https://doi.org/10.3389/fmars.2022.887240

Chen, H., Tseng, Y., Huang, J., & Juang, P. (2025). Understanding the driving mechanisms behind triple-dip La Niñas: insights from the prediction perspective. *Npj Climate and Atmospheric Science*, 8(1). https://doi.org/10.1038/s41612-025-01004-0

Ciardullo, G., Primavera, L., Ferrucci, F., Lepreti, F., & Carbone, V. (2025). Remote-Sensed Spatio-Temporal Study of the Tropical Cyclone Freddy Exceptional Case. *Remote Sensing*, 17(6), 981. https://doi.org/10.3390/rs17060981

Dac Da, N., Foltz, G. R., Balaguru, K., & Fernald, E. (2023). Stronger tropical Cyclone–Induced ocean cooling in Near-Coastal regions compared to the Open Ocean. *Journal of Climate*, 36(18), 6447–6463. https://doi.org/10.1175/jcli-d-22-0842.1

Dare, R. A., & McBride, J. L. (2011). Sea surface temperature response to tropical

cyclones. *Monthly Weather Review*, 139(12), 3798–3808. https://doi.org/10.1175/mwr-d-10-05019.1

Donlon, C. J., Martin, M., Stark, J., Roberts-Jones, J., Fiedler, E., & Wimmer, W. (2011). The Operational Sea Surface Temperature and Sea Ice Analysis (OSTIA) system. *Remote Sensing of Environment*, 116, 140–158. https://doi.org/10.1016/j.rse.2010.10.017

Efendi, U., Fadlan, A., & Hidayat, A. M. (2018). Chlorophyll-A variability in the southern coast of Java Island, Indian Ocean: corresponding to the tropical cyclone of Ernie. *IOP Conference Series Earth and Environmental Science*, 162, 012035. https://doi.org/10.1088/1755-1315/162/1/012035

Feng, M., Zhang, N., Liu, Q., & Wijffels, S. (2018). The Indonesian throughflow, its variability and centennial change. *Geoscience Letters*, 5(1). https://doi.org/10.1186/s40562-018-0102-2

Gonçalves-Araujo, R., Rabe, B., Peeken, I., & Bracher, A. (2018). High colored dissolved organic matter (CDOM) absorption in surface waters of the central-eastern Arctic Ocean: Implications for biogeochemistry and ocean color algorithms. *PLoS ONE*, 13(1), e0190838. https://doi.org/10.1371/journal.pone.0190838

Good, S., Fiedler, E., Mao, C., Martin, M. J., Maycock, A., Reid, R., et al. (2020). The current configuration of the OSTIA system for operational production of foundation sea surface temperature and ice concentration analyses. *Remote Sensing*, 12(4), 720. https://doi.org/10.3390/rs12040720

Hadi, T., Marfai, M. A., & Yuliadi, L. (2019). Climate change impact on tropical cyclone-induced coastal hazards in southern Java, Indonesia. *Natural Hazards*, 95(1), 165–182. https://doi.org/10.1007/s11069-018-3485-2

Hegermiller, C. A., & Thomson, J. (2025). Observations of wave development in gusty winds. *Geophysical Research Letters*, 52(18). https://doi.org/10.1029/2025gl116863

Hendra, A., Kurniawan, A., & Setiawan, I. (2020). Analysis of tropical cyclone influence on sea wave characteristics in the southern waters of Java. *IOP Conference Series: Earth and Environmental Science*, 448(1), 012025. https://doi.org/10.1088/1755-1315/448/1/012025

Huang, A. T., Gillett, Z. E., & Taschetto, A. S. (2024). Australian rainfall increases during Multi-Year La Niña. *Geophysical Research Letters*, 51(9). https://doi.org/10.1029/2023gl106939

Jean-Michel, L., Eric, G., Romain, B., Gilles, G., Angélique, M., Marie, D., et al. (2021). The Copernicus Global 1/12° Oceanic and Sea Ice GLORYS12 Reanalysis. *Frontiers in Earth Science*, 9. https://doi.org/10.3389/feart.2021.698876

Jullien, S., Aucan, J., Kestenare, E., Lengaigne, M., & Menkes, C. (2024). Unveiling the global influence of tropical cyclones on extreme waves approaching coastal areas. *Nature Communications*, 15(1). https://doi.org/10.1038/s41467-024-50929-2

Karnauskas, K. B., Zhang, L., Emanuel, K. A. (2021). The feedback of cold wakes on tropical cyclones. *Geophysical Research Letters*, 48(7). https://doi.org/10.1029/2020gl091676

Kok, P. H., Akhir, M. F. M., Tangang, F., & Husain, M. L. (2017). Spatiotemporal trends in the southwest monsoon wind-driven upwelling in the southwestern part of the South China Sea. *PLoS ONE*, 12(2), e0171979. https://doi.org/10.1371/journal.pone.0171979

Kropf, C. M., Vaterlaus, L., Bresch, D. N., & Pellissier, L. (2025). Tropical cyclone risk for global ecosystems in a changing climate. *Nature Climate Change*. https://doi.org/10.1038/s41558-024-02194-w

Kutsuwada, K. (1998). Impact of wind/wind-stress field in the North Pacific constructed by ADEOS/NSCAT data. *Journal of Oceanography*, 54(5), 443–456. https://doi.org/10.1007/bf02742447

Lellouche, J., Galloudec, O. L., Drévillon, M., Régnier, C., Greiner, E., Garric, G., et al. (2013). Evaluation of global monitoring and forecasting systems at Mercator Océan. *Ocean Science*, 9(1), 57–81. https://doi.org/10.5194/os-9-57-2013

Li, Y., Tang, D. (2022). Tropical cyclone

Wind Pump induced chlorophyll-a enhancement in the South China Sea: A comparison of the open sea and continental shelf. *Frontiers in Marine Science*, 9. https://doi.org/10.3389/fmars.2022.1039824

Li, X., Hu, Z., McPhaden, M. J., Zhu, C., & Liu, Y. (2023). Triple-Dip La Niñas in 1998–2001 and 2020–2023: Impact of mean state changes. *Journal of Geophysical Research Atmospheres*, 128(17). https://doi.org/10.1029/2023jd038843

Li, L., Chan, J. C. L., Wang, G., & Zheng, Y. (2025). Increasing tropical cyclone residence time along the Chinese coastline driven by track rotation. *Npj Climate and Atmospheric Science*, 8(1). https://doi.org/10.1038/s41612-025-01178-7

Lin, J., Ho, H., Gopalakrishnan, G., Zheng, Z., Tseng, R., Pan, J., Ho, C., & Zheng, Q. (2025). Typhoon induced mesoscale cyclonic eddy a long neglected linkage between atmosphere ocean and climate. *Npj Climate and Atmospheric Science*, 8(1). https://doi.org/10.1038/s41612-025-00946-9

Ling, Z., Chen, Z., Wang, G., He, H., & Chen, C. (2021). Recovery of tropical cyclone induced SST cooling observed by satellite in the Northwestern Pacific Ocean. *Remote Sensing*, 13(18), 3781. https://doi.org/10.3390/rs13183781

Liu, H., Satoh, M., Gu, J., Lei, L., Tang, J., Tan, Z., Wang, Y., & Xu, J. (2023). Predictability of the Most Long-Lived Tropical cyclone Freddy (2023) during its westward journey through the southern tropical Indian Ocean. *Geophysical Research Letters*, 50(20). https://doi.org/10.1029/2023gl105729

Liu, Y., Tang, D., Tang, S., Morozov, E., Liang, W., & Sui, Y. (2020). A case study of Chlorophyll a response to tropical cyclone Wind Pump considering Kuroshio invasion and air-sea heat exchange. *The Science of the Total Environment*, 741, 140290. https://doi.org/10.1016/j.scitotenv.2020.140290

Lubis, M. Z., Situmorang, E., Simanjuntak, A. V., Riama, N. F., Pasma, G. R., Dwinovantyo, A., et al. (2025). Indonesian Throughflow, spatial–temporal variability, and its relationship to ENSO events in the Lombok Strait. *The Egyptian Journal of Aquatic Research*. https://doi.org/10.1016/j.ejar.2025.01.004

Ma, Z., Zhang, Z., Fei, J., & Wang, H. (2021). Imprints of tropical cyclones on structural characteristics of mesoscale oceanic eddies over the Western North Pacific. *Geophysical Research Letters*, 48, e2021GL092601. https://doi.org/10.1029/2021GL092601

McTaggart-Cowan, R., Davies, E. L., Fairman, J. G., Galarneau, T. J., & Schultz, D. M. (2015). Revisiting the 26.5°C sea surface temperature threshold for tropical cyclone development. *Bulletin of the American Meteorological Society*, 96(11), 1929–1943. https://doi.org/10.1175/bams-d-13-00254.1

Mears, C. A., Scott, J., Wentz, F. J., Ricciardulli, L., Leidner, S. M., Hoffman, R., & Atlas, R. (2019). A Near-Real-Time version of the Cross-Calibrated Multiplatform (CCMP) ocean surface wind velocity data set. *Journal of Geophysical Research Oceans*, 124(10), 6997–7010. https://doi.org/10.1029/2019jc015367

Ningsih, N. S., Sakina, S. L., Susanto, R. D., & Hanifah, F. (2021). Simulated zonal current characteristics in the southeastern tropical Indian Ocean (SETIO). *Ocean Science*, 17(4), 1115–1140. https://doi.org/10.5194/os-17-1115-2021

Pattie, L. (2022). Tropical Cyclone Paddy. Commonwealth of Australia. https://www.bom.gov.au

Perry, Z., Rapolaki, R., Roffe, S., & Ragoasha, M. (2024). Analysing the atmospheric-oceanic conditions driving the sustained long track and intensity of Tropical Cyclone Freddy. *Tropical Cyclone Research and Review*. https://doi.org/10.1016/j.tcrr.2024.11.008

Pillay, M. T., & Fitchett, J. M. (2021). On the conditions of formation of Southern Hemisphere tropical cyclones. *Weather and Climate Extremes*, 34, 100376. https://doi.org/10.1016/j.wace.2021.100376

Pillay, M. T., & Fitchett, J. M. (2020). Southern hemisphere tropical cyclones: A critical analysis of regional characteristics.

International Journal of Climatology, 41(1), 146–161. https://doi.org/10.1002/joc.6613

Sahoo, B., & Bhaskaran, P. K. (2017). A comprehensive data set for tropical cyclone storm surge-induced inundation for the east coast of India. *International Journal of Climatology*, 38(1), 403–419. https://doi.org/10.1002/joc.5184

Sathyendranath, S., Brewin, R., Brockmann, C., Brotas, V., Calton, B., Chuprin, A., et al. (2019). An Ocean-Colour time series for use in climate studies: The experience of the Ocean-Colour Climate Change Initiative (OC-CCI). *Sensors*, 19(19), 4285. https://doi.org/10.3390/s19194285

Setiawan, R. Y., Susanto, R. D., Wirasatriya, A., Alifdini, I., Puryajati, A. D., Maslukah, L., & Nurdin, N. (2021). Impacts of tropical cyclone Seroja on the phytoplankton chlorophyll-A and sea surface temperature in the Savu Sea, Indonesia. *IEEE Access*, 9, 152938–152944. https://doi.org/10.1109/access.2021.3125605

Shi, H., Chen, Y., Zhao, H., Mortimer, R., & Pan, G. (2025). Impact of tropical cyclone on coastal phytoplankton blooms and underlying mechanisms. *Journal of Hydrology Regional Studies*, 59, 102389. https://doi.org/10.1016/j.ejrh.2025.102389

Sun, Y., Zhong, Z., Li, T., Yi, L., & Shen, Y. (2021). The slowdown tends to be greater for stronger tropical cyclones. *Journal of Climate*, 1–43. https://doi.org/10.1175/jcli-d-20-0449.1

Susilohadi, H., Purnawan, S., & Syamsudin, M. L. (2018). Wave height variability in southern Java waters related to tropical cyclone activity in the Indian Ocean. *Marine Georesources & Geotechnology*, 36(5), 567–575. https://doi.org/10.1080/1064119X.2017.1376135

Suzuki, N., Konda, M., Kutsuwada, K., & Utsunomiya, K. (2018). Comparison of the accuracy of various global wind speed datasets obtained from satellites and reanalyses. *Journal of Advanced Marine Science and Technology Society/Kaiyo Riko Gakkaishi*, 24(2), 31–37. https://doi.org/10.14928/amstec.24.2_31

Tory, K. J., & Dare, R. A. (2015). Sea surface temperature thresholds for tropical cyclone formation. *Journal of Climate*, *28*(20), 8171–8183. https://doi.org/10.1175/jcli-d-14-00637.1

Wang, J., Guo, B., Ji, Z., Che, Y., & Mantravadi, V. S. (2023). Effects of typhoon chanthu on marine chlorophyll A, temperature and salinity. *Atmosphere*, 14(10), 1505. https://doi.org/10.3390/atmos14101505

Wang, Y. (2020). Composite of Typhoon-Induced sea surface temperature and chlorophyll-A responses in the South China Sea. *Journal of Geophysical Research Oceans*, 125(10). https://doi.org/10.1029/2020jc016243

Wen, C., Wang, Z., Wang, J., Li, H., Shi, X., Gao, W., & Huang, H. (2023). Variation of the coastal upwelling off South Java and their impact on local fishery resources. *Journal of Oceanology and Limnology*, 41(4), 1389–1404. https://doi.org/10.1007/s00343-022-2031-3

Wijaya, Y. J., Wisha, U. J., Maslukah, L., Windarto, S., Wirasatriya, A., & Zainuri, M. (2024). Seasonal variation of chlorophyll-a in South Java over the past quarter-century. *Ocean Dynamics*, 74(8), 703–724. https://doi.org/10.1007/s10236-024-01629-4

Wijaya, Y. J., Wisha, U. J., Rejeki, H. A., & Ismunarti, D. H. (2023). Variability of the South Java Current from 1993 to 2021, and its relationship to ENSO and IOD events. *Asia-Pacific Journal of Atmospheric Sciences*, 60(1), 65–79. https://doi.org/10.1007/s13143-023-00336-2

Wirasatriya, A., Setiawan, J. D., Sugianto, D. N., Rosyadi, I. A., Haryadi, H., Winarso, G., et al. (2020). Ekman dynamics variability along the southern coast of Java revealed by satellite data. *International Journal of Remote Sensing*, *41*(21), 8475–8496. https://doi.org/10.1080/01431161.2020.1797215

Yan, X., Ma, Z., Chen, Y., Zheng, Y., & Fei, J. (2025). The e-folding Recovery Time of Tropical Cyclones' Cold Wakes. *Journal of Physical Oceanography*. https://doi.org/10.1175/jpo-d-24-0064.1

Yang, C., Yang, Y. J., Tseng, Y., Jan, S., Chang, M., Wei, C., & Terng, C. (2024). Observational evidence of overlooked

downwelling induced by tropical cyclones in the open ocean. *Scientific Reports*, 14(1). https://doi.org/10.1038/s41598-023-51016-0

Young, I. R. (1999). Wind generated ocean waves. *In Elsevier ocean engineering book series/Elsevier ocean engineering series*. https://doi.org/10.1016/s1571-9952(99)x8001-9

Yu, J., Lv, H., Tan, S., & Wang, Y. (2023). Tropical Cyclone-Induced sea surface temperature responses in the northern Indian Ocean. *Journal of Marine Science and Engineering*, 11(11), 2196. https://doi.org/10.3390/jmse11112196

Zhang, L., & Oey, L. (2018). An observational analysis of ocean surface waves in tropical cyclones in the Western North Pacific Ocean. *Journal of Geophysical Research Oceans*, 124(1), 184–195. https://doi.org/10.1029/2018jc014517

Zhao, H., Pan, J., Han, G., Devlin, A. T., Zhang, S., & Hou, Y. (2017). Effect of a fast-moving tropical storm Washi on phytoplankton in the northwestern South China Sea. *Journal of Geophysical Research Oceans*, 122(4), 3404–3416. https://doi.org/10.1002/2016jc012286

Zu, Y., Fang, Y., Sun, S., Yang, G., Gao, L., & Duan, Y. (2022). The Seasonality of Mesoscale Eddy Intensity in the Southeastern Tropical Indian Ocean. *Front. Mar. Sci.* 9:855832. https://doi.org/10.3389/fmars.2022.855832